

Substrate-induced gliding in a nematic liquid crystal layer

E. Mema, L. Kondic, and L. J. Cummings

*Department of Mathematical Sciences and Center for Applied Mathematics and Statistics,
New Jersey Institute of Technology, Newark, New Jersey 07102, USA*

(Received 16 August 2015; published 28 December 2015)

We consider the interaction between nematic liquid crystals (NLCs) and polymer substrates. Such substrates can interact with NLCs, exhibiting a phenomenon known as director gliding: the preferred orientation of the NLC molecules at the interface changes on time scales that are slow relative to the elastic relaxation time scale of the NLC. We present two models for gliding, inspired by experiments that investigate the interaction between the NLC and a polymer substrate. These models, though simple, lead to nontrivial results, including loss of bistability under gliding. Perhaps surprisingly, we find that externally imposed switching between the steady states of a bistable system may reverse the effect of gliding, preventing loss of bistability if switching is sufficiently frequent. Our findings may be of relevance to a variety of technological applications involving liquid crystal devices, and particularly to a new generation of flexible liquid crystal displays that implement polymeric substrates.

DOI: [10.1103/PhysRevE.92.062513](https://doi.org/10.1103/PhysRevE.92.062513)

PACS number(s): 42.70.Df, 61.30.Dk, 61.30.Gd, 61.30.Hn

I. INTRODUCTION

The interaction between nematic liquid crystals (NLCs) and substrates is of great importance due to the widespread use of portable electronic devices that use liquid crystal displays (LCDs) [1,2]. A typical LCD consists of pixels, within each of which is a thin layer of NLCs placed between two plates a few microns apart [3]. In such devices, the amount of light passing through the layer depends on the orientation of NLC molecules, represented mathematically by a unit vector referred to as the *director field*. This orientation in turn depends both on boundary effects at the plates (NLC molecules have a preferred orientation at solid boundaries, a phenomenon known as *anchoring*) and on external forces (due, in conventional display devices, to an applied electric field). Broadly speaking, the “field on” and “field off” states are optically distinct, giving the basis for a controllable display [4].

Anchoring may be weak or strong, depending on the strength of the interaction between the molecules of the NLC and those of the alignment material at each substrate. For both weak and strong anchoring, the substrate is characterized by an “easy axis,” the axis along which the interaction energy between the substrate and the liquid crystal is minimized. In the case of strong anchoring, the “easy axis” is nearly parallel to the director alignment at the bounding surface. For weak anchoring, the director alignment may deviate significantly from the easy axis, giving rise to a surface torque, which is balanced by the internal elastic torque at the liquid crystal interface [5,6]. At the interface between a NLC and a polymeric substrate, a continuous realignment of the easy axis may occur, typically on a characteristic time scale that is much longer than that of the elastic response of the NLC film. Such a phenomenon has been called director gliding [6,7]: polymeric surfaces are particularly prone to exhibiting this behavior. Director gliding at an interface arises as a result of prolonged exposure to an external force due, e.g., to an applied electric or magnetic field or to the bulk elastic distortion induced by different anchoring conditions (specifically different anchoring angles, although anchoring strength may also differ) at the two bounding interfaces of a NLC layer [8–11].

Studying how director gliding affects the behavior of NLCs is also of relevance due to recent developments in the LCD industry regarding the design of flexible devices, where bounding surfaces are polymeric [1]. Such devices offer significant advantages over glass-based devices (lightweight, unbreakable, flexible) provided that surface effects, including possible gliding, can be well-controlled. We note that, in most liquid crystal display applications, the liquid crystal is not exposed to the bare substrate surface; the substrates are coated with an alignment material (usually mostly organic). The anchoring (and thus the gliding, where it occurs) is really a property of the alignment material, not of the substrate, and it is prevalent in polymer-coated substrates. In the following, however, we do not always make this distinction, and we will refer simply to the anchoring properties of the substrate under gliding. For a polymer-based display based on conventional LCD technology, if anchoring conditions are the same at both bounding surfaces, then the field-free state has very low elastic energy (it should be more or less uniform) and should induce no gliding. With the electric field applied, however, surface molecules experience significant torque, and gliding could occur if the field is sustained for times comparable to the gliding time scale. (Gliding should not, however, be an issue for such devices in only short-term or intermittent use.)

Another situation in which gliding could be an issue is in polymer-based devices that use *bistable* technology [3,12–16]. In a bistable device, the NLC layer can sustain two stable field-free director configurations that are optically distinct in the absence of an applied field. In contrast to a conventional LCD display, an electric field is applied across the layer for the sole purpose of switching between the two director configurations, reducing the power consumption of the LCD device. Bistability exists regardless of whether gliding is present, but such systems may be prone to gliding with soft substrates. To achieve such bistability, the two bounding surfaces must have different anchoring properties, which means that each of the stable states is associated with significant bulk elastic energy, leading to surface torques at the NLC/polymer interface, and hence to gliding over long time scales.

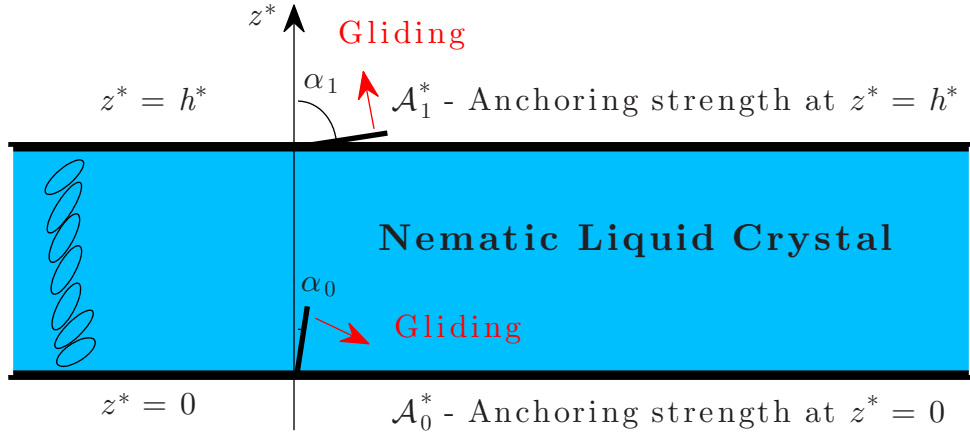


FIG. 1. (Color online) Sketch showing the setup and summarizing the key parameters in dimensional coordinates.

With such considerations in mind, in this paper we develop a mathematical model describing a NLC layer sandwiched between two parallel bounding plates, with different anchoring conditions at each plate, where we assume gliding can occur. Although the phenomenon of gliding may occur in both strongly and weakly anchored systems, our model focuses on gliding in the presence of weak anchoring only, and it may require modification before it can be applied to a system with strong anchoring. Furthermore, we focus on gliding of the zenithal (or polar) director angle only, as observed in, e.g., [7]. We introduce two possible gliding submodels, and we study the effect of each on the director. Although the effect of an applied electric field on gliding is clearly of relevance, we believe that gliding should be first understood precisely in the absence of the field, and that is the focus of this paper. We consider the simplest case in which the director is confined to a plane perpendicular to the bounding plates: this, together with our neglect of the dielectric and flexoelectric contributions in the free-energy density, permits an analytical solution for the director. In line with what is known about the relative time scales of gliding and director reorientation in the bulk, we consider a quasistatic model in which the director angle, θ , depends on time only via the changes in anchoring angles on the long (gliding) time scale. The model we use permits bistability, and therefore we study this aspect of the system under gliding also.

The paper is laid out as follows: In Sec. II we introduce the key variables, discuss the modeling assumptions, and present the equations used to govern the evolution of the director field and the anchoring angles at each surface. One of our modeling assumptions for gliding is that, due to the properties of the polymeric bounding plates, the anchoring angle cannot change by an arbitrarily large amount from its initial value [6,8]: we limit the change by some prescribed tolerance value, θ_{tol} . This assumption is supported by the experimental results reported by Jánossy and Kósa [6] and Joly *et al.* [7]. Section II A discusses two possible ways to implement this: (i) gliding is stopped abruptly when the tolerance is reached; (ii) gliding stops smoothly as θ_{tol} is approached. Section III presents the results for the two models, and Sec. IV discusses conclusions to be drawn and future work.

II. MATHEMATICAL MODEL

Figure 1 shows the basic setup that consists of a nematic liquid crystal layer placed between two parallel bounding plates at $z^* = 0$ and $z^* = h^*$. Here, superscripts are used to denote dimensional quantities; they will be dropped when nondimensionalizing. The local average molecular orientation throughout the layer is described by a unit vector director field, \mathbf{n} , which we assume lies in the (x^*, z^*) plane, but it does not depend on x^* . Hence, we consider a one-dimensional model in which the director can be expressed in terms of a single angle, $\theta(z^*) \in (-\pi/2, \pi/2]$, the angle the director makes with the z^* axis: $\mathbf{n} = (\sin \theta, 0, \cos \theta)$. This assumption obviously limits our investigation to gliding of the zenithal or polar director angle only (as observed in [7]), although we note that gliding of the director azimuthal angle may certainly occur in systems with twist, e.g., [6]. In addition, we consider a steady-state model, reflecting the assumption that the elastic response of the NLC layer is established in milliseconds [7], much faster than the time scale on which director gliding occurs (minutes to hours [6,7,10,11,17]).

The free energy of the liquid crystal layer, in the absence of an applied electric field and with specified anchoring conditions at each bounding surface, includes both bulk and surface contributions. The bulk free-energy density W^* comprises splay and bend elastic contributions (since the director is confined to a plane, there is no twist), and with the assumed form for \mathbf{n} and the frequently used assumption of equal bend and splay elastic constants, $K_1^* = K_2^* = K_3^* = K^*$ [18,19], it is given by

$$W^* = \frac{K^*}{2} \theta_{z^*}^2. \tag{1}$$

We focus on weak anchoring conditions since we expect that, particularly in this case, interesting dynamics arise as a result of the energy minimization between the substrate and the liquid crystal. The total free energy of the system comprising both bulk and surface energy contributions is then given as

$$J^* = \int_0^{h^*} W^* dz^* + g_0^*|_{z^*=0} + g_{h^*}^*|_{z^*=h^*}, \tag{2}$$

where $g_{\{0,h^*\}}^*$ (at $z^* = 0, h^*$) are the Rapini-Papoular surface energies used to model the surface anchoring at each boundary [20]. They are given by $g_{\{0,h^*\}}^* = \mathcal{A}_{\{0,h^*\}}^* \sin^2(\theta - \alpha_{\{0,h^*\}})$, where $\alpha_{\{0,h^*\}}$ are the preferred anchoring angles at $z^* = 0, h^*$, respectively, and $\mathcal{A}_{\{0,h^*\}}^*$ are the anchoring strengths. An accurate description of the dynamic process by which the director evolves to minimize the free energy given by Eq. (2) requires the full equations of nematodynamics that couple flow and director orientation [18,21]. We follow several authors (e.g., Davidson and Mottram [3], Cummings *et al.* [12,13], and Kedney and Leslie [14]) in assuming that the system evolves in the direction that minimizes its total free energy (a gradient flow). This approach leads to the following time-dependent problem:

$$\begin{aligned} \tilde{\mu}^* \theta_{t^*} &= K^* \theta_{z^* z^*}, \\ \tilde{\nu}^* \theta_{t^*} &= K^* \theta_{z^*} - \frac{\mathcal{A}_0^*}{2} \sin 2(\theta - \alpha_0) \quad \text{on } z^* = 0, \\ -\tilde{\nu}^* \theta_{t^*} &= K^* \theta_{z^*} + \frac{\mathcal{A}_1^*}{2} \sin 2(\theta - \alpha_{h^*}) \quad \text{on } z^* = h^*, \end{aligned} \quad (3)$$

where $\tilde{\mu}^*$ and $\tilde{\nu}^*$ are bulk and surface rotational viscosities, respectively. In the following, we supplement Eqs. (3) by two proposed gliding models that capture the dynamics of molecular reorientation under gliding, before nondimensionalizing and simplifying the resulting full system.

A. Gliding

Fundamentally, the anchoring properties of a given polymer surface are due to the orientation of its molecules at the exposed polymer surface and their interactions with the molecules of the NLC. At a nongliding surface, the preferred orientation of the molecules is fixed, as dictated by the anchoring conditions. At a gliding surface, by contrast, the molecules can slowly reorient in time if there is a sustained torque on them due to the molecules of the adjacent NLC. Such a torque arises, for example, if the anchoring conditions within our NLC layer are different at the two bounding surfaces, leading to a director orientation that changes across the layer, with attendant elastic stress throughout the layer (including at the bounding surfaces). Such molecular torques at the bounding surfaces lead to slow variation of the anchoring angles in time: experimentally, the anchoring angle is observed to reorient toward the director angle at that surface [5–8,10,11,17]. We introduce two models to capture this gliding behavior. Both models assume that the rate of anchoring reorientation at a

surface depends on the difference between the anchoring angle and the director angle at that surface.

The models also incorporate an additional feature, observed in experiments such as those of Jánossy and Kósa [6] and Joly *et al.* [7]: gliding does not continue indefinitely; rather, the anchoring angle stops reorienting after some time under torque. The experimental setup used in [6] consists of a nematic liquid crystal layer placed between two different substrates, only one of which exhibits gliding (azimuthal gliding, rather than the zenithal or polar gliding that we model). Anchoring is strong and planar (aligned with a specific rubbing direction) at the upper (nongliding) substrate, and it is weak and planar at the lower substrate, where gliding occurs. The layer is exposed to a magnetic field applied perpendicular to the rubbing direction. The anchoring angle at the lower substrate rotates (glides) in time under the magnetic torque. The field is removed after some time (before any steady state is reached, but after significant gliding), and the system is then allowed to evolve under gliding alone. If gliding were unlimited, the system would ultimately glide back to a fully undistorted state throughout the layer, this being the global energy minimizer. However, this does not happen, indicating that there is some physical constraint on the degree of gliding that can occur. (Similar observations regarding limited gliding were made by Joly *et al.* [7], although with a slightly different setup.)

Jánossy and Kósa interpreted their experimental results by developing a model based on the \mathbf{Q} -tensor formulation for nematics [6,18]. Although their model is in very good agreement with the experimental results over reasonable times, it does not capture the fact that the surface director appears not to relax back to its original state in the experiments. By contrast, we base our governing equations on the Ericksen-Leslie theory for nematic liquid crystals. In addition, we account for the observed limited gliding described above by introducing the parameter θ_{tol} , as explained in detail below.

1. Gliding model I: Abrupt cessation

In the first gliding model, we assume that the anchoring angle, α , changes at a rate directly proportional to its deviation from the adjacent director angle. The anchoring reorientation (gliding) persists until the anchoring angle has changed by a maximal amount θ_{tol} or until $\theta(\cdot, t^*) = \alpha_{\{0,h^*\}}(t^*)$, at which point gliding stops abruptly. Mathematically, this is represented as follows:

$$\frac{d\alpha_{\{0,h^*\}}}{dt^*} = \begin{cases} \lambda_{\{0,h^*\}}^* [\theta(\cdot, t^*) - \alpha_{\{0,h^*\}}(t^*)] & \text{if } |\alpha_{\{0,h^*\}}(t^*) - \alpha_{\{0,h^*\}}(0)| < \theta_{\text{tol}}, \\ 0 & \text{if } |\alpha_{\{0,h^*\}}(t^*) - \alpha_{\{0,h^*\}}(0)| = \theta_{\text{tol}}, \end{cases} \quad (4)$$

where $\theta(\cdot, t^*)$ indicates that $\theta(z^*, t^*)$ is evaluated at the appropriate boundary. Here, $\lambda_{\{0,h^*\}}^*$ are the anchoring relaxation rates at $z^* = 0, h^*$, respectively. When $\theta_{\text{tol}} = 0$, the interface exhibits no gliding, while as $\theta_{\text{tol}} \rightarrow \pi/2$ the gliding process occurs indefinitely, as in the model described in [6]. Unlimited gliding leads ultimately to a director that is uniform throughout the layer, although this uniform value is

unknown *a priori* and will depend on the relative values of the anchoring relaxation rate constants at the two boundaries. The model given by Eq. (4) introduces gliding in perhaps the simplest possible manner; we will use this simplicity below to gain a better understanding of the basic features of gliding. Before doing so, we introduce our second gliding model.

2. Gliding model II: Smooth cessation

Model I has the advantage of maximal simplicity, but it has the perhaps unrealistic feature that gliding halts abruptly once gliding through angle θ_{tol} has occurred. We therefore propose a second gliding model (model II) with the same essential features as model I, but here we ensure smooth cessation of gliding by specifying the rate of change of the anchoring angles according to

$$\frac{d\alpha_{\{0,h^*\}}}{dt^*} = \lambda_{\{0,h^*\}}^* [\theta(\cdot, t^*) - \alpha_{\{0,h^*\}}(t^*)] \times \left(1 - \frac{|\alpha_{\{0,h^*\}}(t^*) - \alpha_{\{0,h^*\}}(0)|}{\theta_{\text{tol}}} \right). \quad (5)$$

Note that the first factor on the right-hand side is present in both models, ensuring that the anchoring angle always reorients itself toward the director angle at that interface. The second term leads, however, to a slowdown of the gliding process as the maximum gliding angle is approached.

B. Scaling and nondimensionalization

We scale z^* with the cell height h^* and define t , the nondimensional time variable, as $t = t^* \lambda_0^*$, where λ_0^* is the relaxation rate associated with the lower substrate $z^* = 0$. Relaxation rates can be inferred from experimental data reported in the literature. We use the results of Janossy and Kosa [6] to estimate $\lambda_{\{0,h^*\}}^*$. Their experiment consists of a nematic liquid crystal layer sandwiched between two polymer plates, where one plate is treated chemically to ensure strong anchoring while the other is left as a “soft” plate, exhibiting weak anchoring with gliding. Modifying our model to account for strong anchoring at the plate, $z^* = h^*$, we are able to obtain good agreement between the experimentally observed evolution of the anchoring angle at the “soft” plate [6] and our model by using $\lambda_0^* \approx 0.0031 \text{ s}^{-1}$ as a relaxation rate in gliding model I. Hence, we assume this value in our nondimensionalization.

The surface energies $g_{\{0,h^*\}}^*$ (at $z^* = 0, h^*$) are nondimensionalized by $g_{\{0,1\}} = g_{\{0,h^*\}}^* h^* / K^*$ leading to the nondimensional Rapini-Papoular surface energies: $g_{\{0,1\}} = (\mathcal{A}_{\{0,1\}}/2) \sin^2(\theta - \alpha_{\{0,1\}})$, $\mathcal{A}_{\{0,1\}} = (h^* \mathcal{A}_{\{0,h^*\}}^*) / K^*$, where $\alpha_{\{0,1\}} \equiv \alpha_{\{0,h^*\}}^*$. Equations (3) in turn become

$$\begin{aligned} \delta\theta_t &= \theta_{zz} & \text{in } & 0 < z < 1, \\ \delta\tilde{v}\theta_t &= \theta_z - \frac{\mathcal{A}_0}{2} \sin 2(\theta - \alpha_0) & \text{on } & z = 0, \\ -\delta\tilde{v}\theta_t &= \theta_z + \frac{\mathcal{A}_1}{2} \sin 2(\theta - \alpha_1) & \text{on } & z = 1, \end{aligned} \quad (6)$$

where $\delta = h^{*2} \tilde{\mu}^* \lambda_0^* / K^*$ and $\tilde{v} = \tilde{v}^* / (\tilde{\mu}^* h^*)$. Note that δ represents the ratio between two time scales: $h^{*2} \tilde{\mu}^* / K^*$ is the time scale of the bulk elastic response of the NLC, while $1/\lambda_0^*$ is the time scale of the gliding response (the estimate above gives a little over 5 min for the gliding response, but this time scale may range from a few minutes to several hours depending on the properties of the liquid crystal and the substrate [6,7,10,11,17]). Typical values of the dimensional parameters are $h^* \sim 1 \times 10^{-6} \text{ m}$, $K^* \sim 1 \times 10^{-12} \text{ N}$, $\tilde{\mu}^* \sim 0.1 \text{ N s m}^{-2}$, $\mathcal{A}_{\{0,h^*\}}^* \sim 10^{-4} - 10^{-6} \text{ N m}^{-1}$, and $\tilde{v}^* \sim 10^{-10} \text{ N s m}^{-1}$ [3,5,22].

Hence the bulk elastic response time scale of the NLC is of the order of a few milliseconds, and $\delta \ll 1$, $\tilde{v} \ll 1$. We therefore use a quasistatic approximation and set $\delta = 0$ in Eqs. (6), giving

$$0 = \theta_{zz}, \quad (7)$$

$$0 = \theta_z - \frac{\mathcal{A}_0}{2} \sin 2(\theta - \alpha_0) \quad \text{on } z = 0, \quad (8)$$

$$0 = \theta_z + \frac{\mathcal{A}_1}{2} \sin 2(\theta - \alpha_1) \quad \text{on } z = 1. \quad (9)$$

The dimensionless forms of the gliding models I and II given by Eqs. (4) and (5) are as follows:

$$\begin{aligned} \text{model I: } & \frac{d\alpha_{\{0,1\}}}{dt} \\ &= \begin{cases} \lambda_{\{0,1\}} [\theta(\cdot, t) - \alpha_{\{0,1\}}(t)] & \text{if } |\alpha_{\{0,1\}}(t) - \alpha_{\{0,1\}}(0)| < \theta_{\text{tol}}, \\ 0 & \text{if } |\alpha_{\{0,1\}}(t) - \alpha_{\{0,1\}}(0)| = \theta_{\text{tol}}; \end{cases} \end{aligned} \quad (10)$$

$$\begin{aligned} \text{model II: } & \frac{d\alpha_{\{0,1\}}}{dt} \\ &= \lambda_{\{0,1\}} [\theta(\cdot, t) - \alpha_{\{0,1\}}(t)] \left(1 - \frac{|\alpha_{\{0,1\}}(t) - \alpha_{\{0,1\}}(0)|}{\theta_{\text{tol}}} \right), \end{aligned} \quad (11)$$

where $\lambda_{\{0,1\}} = \lambda_{\{0,h^*\}}^* / \lambda_0^*$ (so $\lambda_0 = 1$ always; in fact, for all simulations shown in this paper we also set $\lambda_1 = 1$). Equations (7)–(9) governing the director orientation will be dynamic once supplemented with the gliding model [Eq. (10) or (11)] describing how $\alpha_{\{0,1\}}$ change in time. Note that the actual gliding time scale, $1/\lambda_0^*$, is important only if we wish to convert our dimensionless results back to real time.

III. ANALYSIS AND RESULTS

A. Solution scheme

Equations (7)–(9) in conjunction with either Eq. (10) or Eq. (11) constitute a complete model to describe the director field angle $\theta(z, t)$ within a simple sandwich of NLC with gliding at both interfaces [dynamic evolution of $\alpha_0(t)$, $\alpha_1(t)$]. Due to the quasistatic approximation, Eqs. (7)–(9) can be solved independently of the gliding model if the anchoring angles $\alpha_{\{0,1\}}$ are assumed known: $\theta = az + b$, where a and b are fixed by Eqs. (8) and (9). Following [13], the director solution may be written as

$$\theta = az + \frac{1}{2} \sin^{-1} \left(\frac{2a}{\mathcal{A}_0} \right) + \alpha_0, \quad (12)$$

where a satisfies a nonlinear algebraic equation,

$$\begin{aligned} f(a) &= a + a \frac{\mathcal{A}_1}{\mathcal{A}_0} \cos[2a + 2(\alpha_0 - \alpha_1)] \\ &+ \frac{\mathcal{A}_1 \sqrt{\mathcal{A}_0^2 - 4a^2}}{2\mathcal{A}_0} \sin[2a + 2(\alpha_0 - \alpha_1)] = 0 \end{aligned} \quad (13)$$

(here the time dependence in a , α_0 , and α_1 is suppressed for brevity). Given the initial conditions $\alpha_0(0)$, $\alpha_1(0)$ for the

anchoring angles and the values \mathcal{A}_0 , \mathcal{A}_1 for the anchoring strengths, Eqs. (12) and (13) describe possible initial states for the system. We choose values of \mathcal{A}_0 and \mathcal{A}_1 that correspond to “weak anchoring” ($\mathcal{A}_{\{0,1\}^*} \sim 10^{-6} \text{ N m}^{-1}$). In addition, we expose any behavior due to different anchoring conditions at each substrate by setting $\mathcal{A}_0 \neq \mathcal{A}_1$: in all simulations presented in this paper, we take $\mathcal{A}_0 = 5.0$, $\mathcal{A}_1 = 2.4$, as used in [13].

Depending on the values of $\{\alpha_0(0), \alpha_1(0)\}$, Eq. (13) may have multiple solutions. For the chosen values of $\mathcal{A}_0, \mathcal{A}_1$, the number of solutions is always one or three, and we will focus on this case in the rest of the paper. Choosing different values of \mathcal{A}_0 and \mathcal{A}_1 , however, may lead to more than three solutions, each of which is associated with a root of Eq. (13). In such cases, the multiple roots of larger amplitude correspond to complex director configurations in which the director bends through large angles. These configurations are unlikely to be observed in physical systems due to the associated high elastic energy, and they will not be considered further. [Such solutions may be considered an artifact of our assumption of purely two-dimensional (2D) geometry: real systems are 3D and the director can “escape” from a highly bent 2D solution, unwinding into the third dimension.] When Eq. (13) has one root, the system has only one steady state (monostability); when it has three roots, the system is bistable (one of the three roots always represents an unstable solution for θ , a local maximum of the free energy).

The results that we present are obtained as follows. From our chosen initial state, integrating either Eq. (10) or Eq. (11) through one time step using the appropriate integrating factor, we compute the evolution of the anchoring angles based on models I and II. These anchoring angles are used to obtain a new director solution using Eqs. (12) and (13) at the new time step. To ensure accuracy, we use a relatively small time step, $dt = 10^{-3}$; we have verified that such dt leads to results that are accurate to 0.1%.

B. Effect of gliding on a monostable system

We focus first on an initially monostable system, and we consider how the proposed gliding models I and II drive the

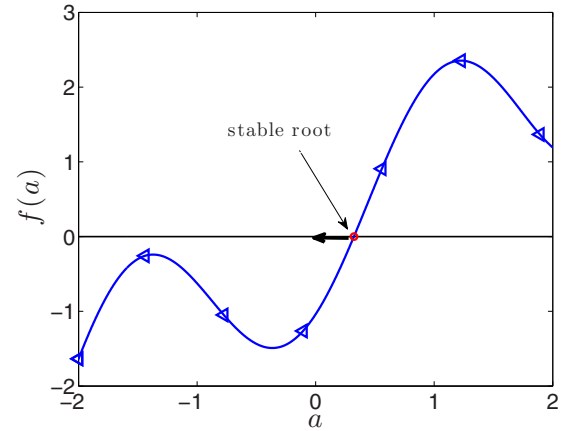


FIG. 2. (Color online) The location of the root of $f(a)$ [see Eq. (13)] for a monostable system. The anchoring angles are $\alpha_0(0) = 0$ and $\alpha_1(0) = \pi/6$. The arrow accompanying the root indicates its initial evolution under gliding (model I). The symbols on the curves shown in this and upcoming figures are purely for identification with the legend.

evolution of the anchoring angles and the director field under unlimited ($\theta_{\text{tol}} = \pi/2$) and limited ($\theta_{\text{tol}} < \pi/2$) gliding (we use $\theta_{\text{tol}} = \pi/20$ as a representative example). We expect unlimited gliding to smooth the director solution throughout the layer, leading to a uniform solution at large time, while limited gliding may lead to a nonuniform steady state for the director.

Figure 2 shows a snapshot of $f(a)$, defined in Eq. (13), for a monostable system. Figure 3(a) shows the evolution of the director field from the initial state represented by the root in Fig. 2 under unlimited gliding. These results are computed using model I; results obtained using model II are very similar and are therefore omitted. Figure 3(b) shows the accompanying evolution of the anchoring angles α_0, α_1 for both gliding models I and II. For both models, with $\theta_{\text{tol}} = \pi/2$, the director field evolves to a solution that is uniform throughout the layer, with $\theta(z, \infty) = \alpha_0(\infty) = \alpha_1(\infty)$. However, the steady states attained by the two models are not the same in Fig. 3(b):

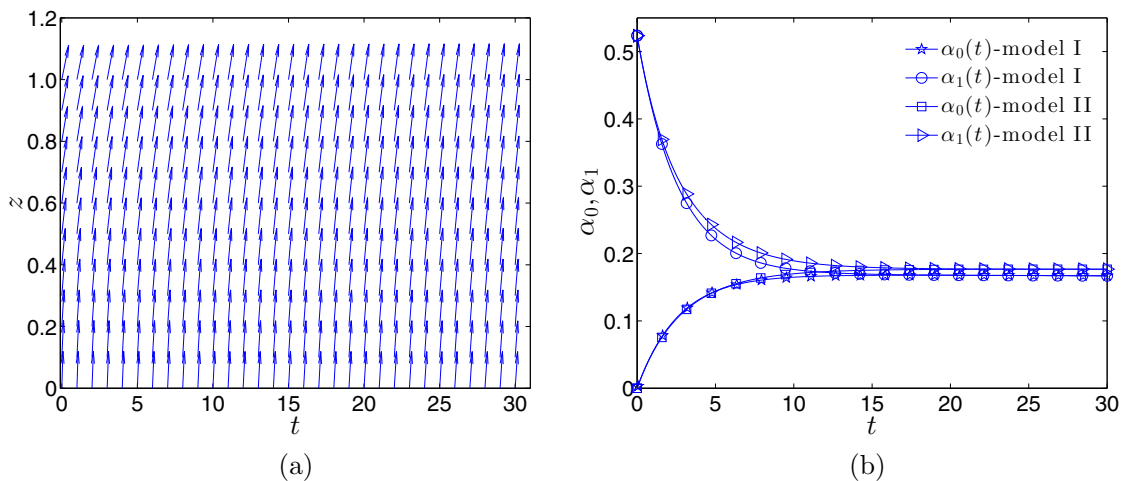


FIG. 3. (Color online) Gliding effect for $\theta_{\text{tol}} = \pi/2$ (unlimited gliding) using models I and II: $\alpha_0(0) = 0$, $\alpha_1(0) = \pi/6$, and $\lambda_0 = \lambda_1 = 1.0$ (these values for the dimensionless relaxation constants are assumed throughout this paper). (a) Evolution of the director field in time as a result of gliding model I. (b) Evolution of anchoring angles for model I: $\alpha_0(t)$ —(★), $\alpha_1(t)$ —(○); and model II: $\alpha_0(t)$ —(□), $\alpha_1(t)$ —(▷).

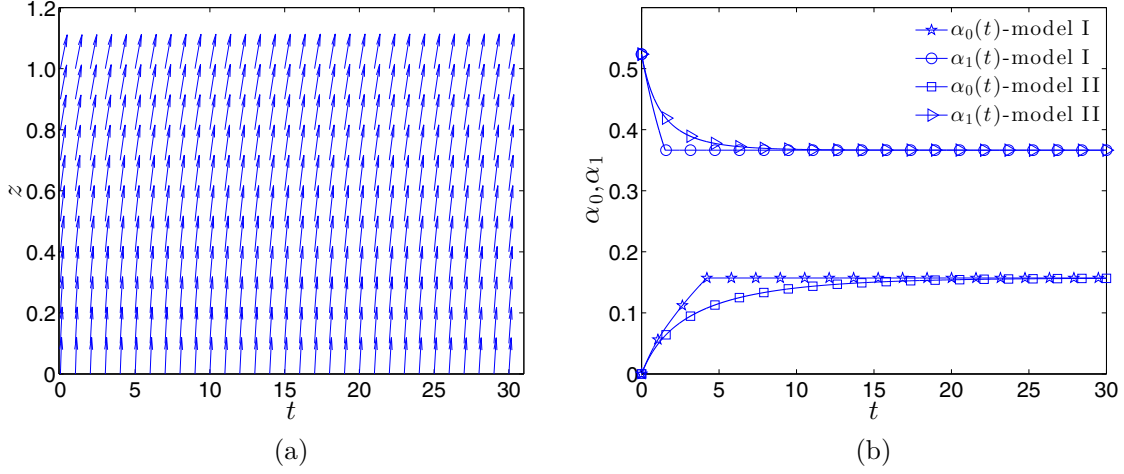


FIG. 4. (Color online) Gliding effect for $\theta_{\text{tol}} = \pi/20$ (limited gliding) using models I and II: $\alpha_0(0) = 0$, $\alpha_1(0) = \pi/6$, and $\lambda_0 = \lambda_1 = 1.0$. (a) Evolution of the director field in time as a result of gliding model I. (b) Evolution of anchoring angles for model I: $\alpha_0(t)$ —(\star), $\alpha_1(t)$ —(\circ); and model II: $\alpha_0(t)$ —(\square), $\alpha_1(t)$ —(\triangleright).

the additional smoothing factor $[1 - |\alpha_{\{0,1\}}(t) - \alpha_{\{0,1\}}(0)|/\theta_{\text{tol}}]$ in Eq. (5) becomes important, leading to quantitatively different results. This observation highlights the importance of accurately capturing the intermediate dynamics in any gliding model. Note also that, regardless of the model used, $\alpha_1(t)$ varies more from its initial value than does $\alpha_0(t)$ due to the lower associated anchoring strength ($\mathcal{A}_0 = 5.0$, $\mathcal{A}_1 = 2.4$).

Figure 4 shows the evolution of the director solution and the anchoring angles under gliding models I and II for $\theta_{\text{tol}} = \pi/20$, with all other parameters as in Fig. 3. We note that the anchoring angles at the two boundaries no longer settle at the same steady-state value: $\alpha_0(\infty) \neq \alpha_1(\infty)$, leading to a director solution that is nonuniform throughout the layer at large times. In addition, we observe that, unlike the unlimited gliding example of Fig. 3, under limited gliding the two models lead to the same steady-state solution at long times, at least for sufficiently small θ_{tol} as used here. This is due to the fact that, for sufficiently small θ_{tol} , gliding stops (for both models) due to the maximum gliding angle being reached: $|\alpha_{\{0,1\}}(t) - \alpha_{\{0,1\}}(0)| = \theta_{\text{tol}}$ at finite time [see Eq. (10) or Eq. (11)].

C. Effect of gliding on a bistable system

The existence of two (or more) stable field-free steady states that are optically distinct is of relevance to applications, since in this case contrast can be maintained in a display without an externally applied electric field (a field is required only to switch the device from one state to the other). Theoretical investigations of bistable devices have been carried out by many authors: see, e.g., [3, 12–14] and references therein. In [12], bistability is obtained in a special case in which the anchoring angles are $\pi/2$ out of phase and the anchoring strengths are the same at both boundaries; switching between the states is obtained through the application of a transient electric field. In particular, two-way switching is possible for weak anchoring only. In [13], Cummings *et al.* generalized the study by treating the anchoring conditions as adjustable parameters, providing the values of $\mathcal{A}_{\{0,1\}}, \alpha_{\{0,1\}}$, for which bistability and switching are possible. In the same spirit,

bistability may be achieved in the simple model considered here by appropriate choice of (initial) anchoring conditions: whether the system remains bistable over long times depends on how the anchoring angles evolve under gliding. In this section, we consider the effect of gliding on bistable systems by means of specific examples.

Figure 5(a) shows an example of the function $f(a)$, defined in Eq. (13), for a bistable system. The roots of this function determine director solutions as in Eq. (12); here $f(a)$ has three roots, only two of which represent stable solutions, as discussed below. With anchoring strengths fixed, we find that whether the system specified by Eqs. (7)–(9) is bistable [three roots of $f(a)$] or monostable [one root of $f(a)$] depends primarily on the difference of the initial anchoring angles, $\Delta\alpha(0) = \alpha_1(0) - \alpha_0(0)$, with only weak dependence on individual values of the two anchoring angles; therefore, for purposes of illustration we set $\alpha_0(0) = 0$ and vary $\alpha_1(0)$. Figure 5(b) shows how the number of solutions of Eqs. (7)–(9) then depends on $\Delta\alpha(0)$. We observe that if $\Delta\alpha(0) = \alpha_1(0) - \alpha_0(0) < \Delta\alpha_c \approx 0.82$, the function $f(a)$, defined by Eq. (13), has only one root, corresponding to a single solution $\mathbf{n} = (\sin\theta, 0, \cos\theta)$, where θ is given by Eq. (12). Two stable steady states emerge if $\Delta\alpha(0) > \Delta\alpha_c$: in this case, $f(a)$ has three roots, two corresponding to stable solutions given by Eq. (12) [local minima of the free energy given in Eq. (2)], and one corresponding to an unstable solution (local maximum of the free energy). Note that the particular value of $\Delta\alpha_c$ in a given system depends also on the anchoring strengths, $\mathcal{A}_{\{0,1\}}$; in Fig. 5, as elsewhere, these are set at $\mathcal{A}_0 = 5.0$, $\mathcal{A}_1 = 2.4$.

1. Effect of unlimited gliding on a bistable system

The discussion presented so far in this section pertains to the initial states of a system before any gliding dynamics are seen. Since gliding can affect the structure of an initially bistable system, we explore its effect below, discussing a specific example. Before doing so, we observe that as the anchoring angles $\alpha_0(t), \alpha_1(t)$ vary under gliding, the function

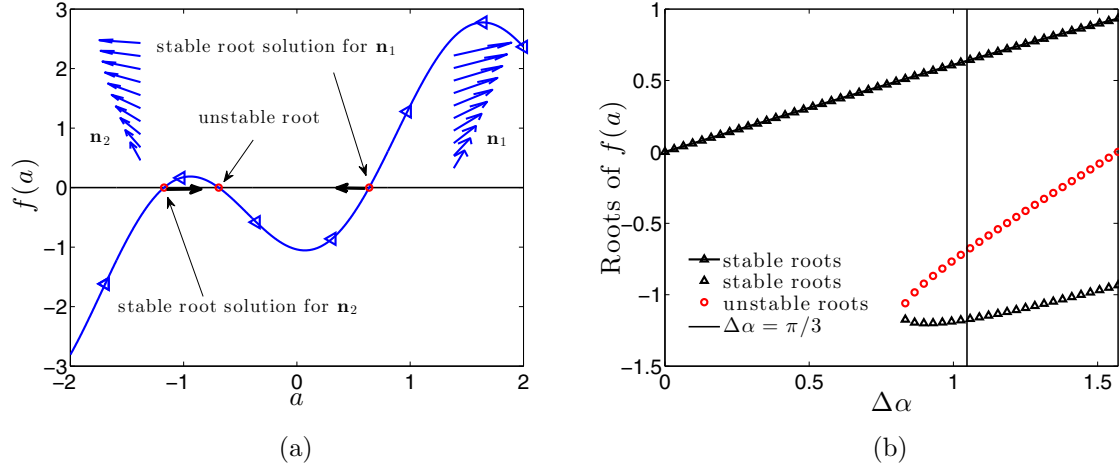


FIG. 5. (Color online) (a) Location of the roots of $f(a)$ for a bistable system with $\alpha_0(0) = 0$, $\alpha_1(0) = \pi/3$. The arrows accompanying the stable roots indicate their initial evolution under gliding. Two steady-state configurations \mathbf{n}_1 and \mathbf{n}_2 are shown, corresponding to $a_1 \approx 0.63$ and $a_2 \approx -1.17$. (b) Dependence of solution multiplicity on $\Delta\alpha = \alpha_1(0) - \alpha_0(0)$, where $\Delta\alpha$ varies from 0 to $\pi/2$ with $\alpha_0(0) = 0$. When $f(a)$ [defined by Eq. (13)] has three roots, two correspond to stable steady states (Δ) and one to an unstable steady state (\circ). The vertical line is drawn at $\Delta\alpha(0) = \pi/3$, the state shown in (a).

$f(a)$ defined by Eq. (13) evolves in time as well. In the following, we say that we “track” \mathbf{n}_1 or \mathbf{n}_2 when the director solution [given by Eq. (12)], whose behavior is dictated by the evolution of the largest or smallest root of $f(a)$, evolves under gliding. It is important to emphasize that this evolution under gliding is totally different for each steady state, as we now discuss.

Given values for the surface energies, \mathcal{A}_0 , \mathcal{A}_1 , and initial values for the anchoring angles, $\alpha_0(0)$, $\alpha_1(0)$, the system has a choice of two steady states, \mathbf{n}_1 or \mathbf{n}_2 , corresponding to two distinct roots of Eq. (13). If we start with state \mathbf{n}_1 and track it under gliding, the anchoring angles will evolve according to the solution of Eq. (10) or Eq. (11). Since each of these equations depends on the director solution \mathbf{n}_1 itself, the evolution here is quite different than if we started from the solution \mathbf{n}_2 .

Note also that, when we track solution \mathbf{n}_1 , the solution \mathbf{n}_2 corresponding to the other (stable) root of $f(a)$ exists “in the background,” but is not manifested. This “background” evolution of \mathbf{n}_2 , when tracking \mathbf{n}_1 , is again quite different from the evolution of \mathbf{n}_2 when it is the solution being tracked. The following explicit examples should clarify these remarks.

Consider the two possible scenarios for the evolution of $f(a)$ in Fig. 5(a) with $\Delta\alpha(0) = \pi/3$. Initially this system has two stable steady states, \mathbf{n}_1 and \mathbf{n}_2 , corresponding to the roots of $f(a)$ as shown in Fig. 5(a). Figures 6(a) and 7(a) show the evolution of the director field when tracking \mathbf{n}_1 and \mathbf{n}_2 , respectively, under unlimited gliding using model I. Similarly to the monostable case, independently of which gliding model we choose, for $\theta_{\text{tol}} = \pi/2$ gliding smooths the solution $\theta(z; t)$ as time progresses, leading ultimately to a director solution that is uniform throughout the domain. Note, however, that, in line with our remarks above, the long-time uniform solution obtained depends on which solution was tracked; compare the final states in Figs. 6(a) and 7(a).

As the steady states \mathbf{n}_1 and \mathbf{n}_2 evolve under gliding toward the uniform state, in either case the system switches from

bistable to monostable. To illustrate how bistability is lost, we show early time evolution of $f(a)$ in Figs. 6(b) and 7(b). We see that in both cases, $f(a)$ evolves in a way that leads to the loss of two roots under gliding, leaving only a single root, corresponding to one stable steady state. Figure 6(b) shows that, while tracking \mathbf{n}_1 , the root corresponding to \mathbf{n}_1 persists in time while the root corresponding to \mathbf{n}_2 disappears at $t \approx 0.6$ [$f(a)$ moves to the left and down]. Similarly, Fig. 7(b) shows that, when tracking \mathbf{n}_2 , the root corresponding to \mathbf{n}_2 persists in time while the root corresponding to \mathbf{n}_1 disappears at $t \approx 2.5$ [$f(a)$ moves to the right and up]. These figures also illustrate that the time at which bistability is destroyed, t_b , depends on which state we are tracking, \mathbf{n}_1 or \mathbf{n}_2 .

As the director solution \mathbf{n}_1 (or \mathbf{n}_2) is tracked under gliding, the director begins to relax and move smoothly toward a uniform state, as in Fig. 6(a) [or Fig. 7(a)]. As this happens, the total energy associated with \mathbf{n}_1 (or \mathbf{n}_2) decreases. At the same time, however, the total energy associated with the other “background” stable state \mathbf{n}_2 (or \mathbf{n}_1) increases, as shown in Fig. 6(c) [or Fig. 7(c)]. If, as is the case in Figs. 6 and 7, gliding is not halted, the energy of that background state, \mathbf{n}_2 (or \mathbf{n}_1), will ultimately increase to a stage where that solution is no longer a local minimum of the free energy [at which point that steady state ceases to exist, simultaneously with the loss of roots of $f(a)$].

In the particular case considered in Figs. 6 and 7, bistability is destroyed faster when tracking \mathbf{n}_1 . This seems to be a consequence of the higher bulk energy associated with the director solution for \mathbf{n}_2 . This solution \mathbf{n}_2 represents a shallower local minimum of the free energy for this parameter set, so that it is destroyed sooner under gliding. Figures 6(c) and 7(c) show the total free energies [given by $J = J^*h^*/K^*$; see Eq. (2)] of both the solution being tracked (solid line) and the “background” solution (dashed line): we see that in both cases the solution being tracked decreases its total free energy under gliding, while the energy of the background solution increases. In these unlimited gliding examples, the dashed line stops abruptly in both cases, corresponding to the loss of the

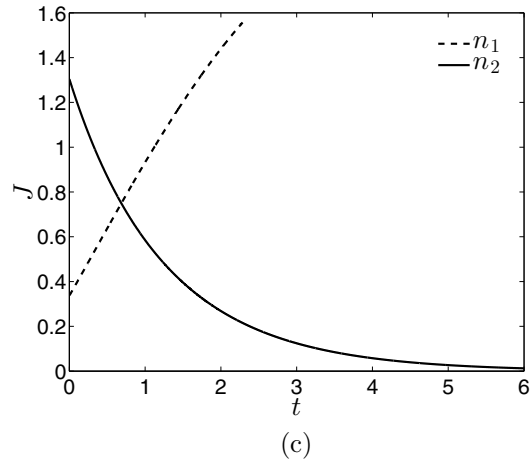
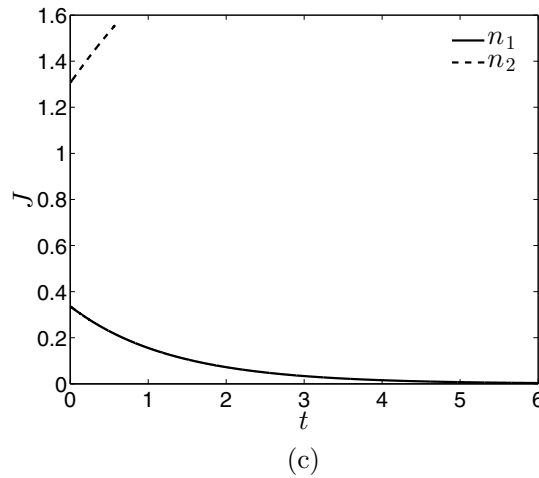
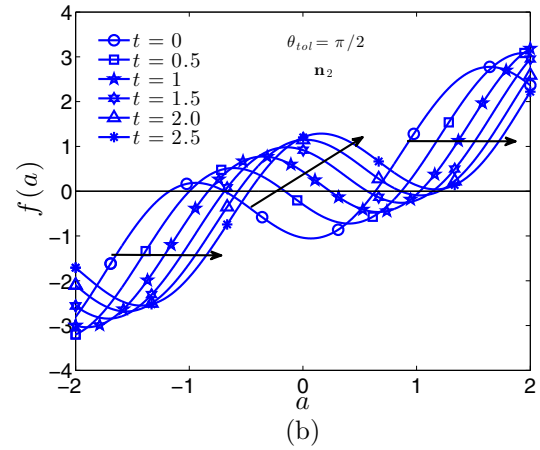
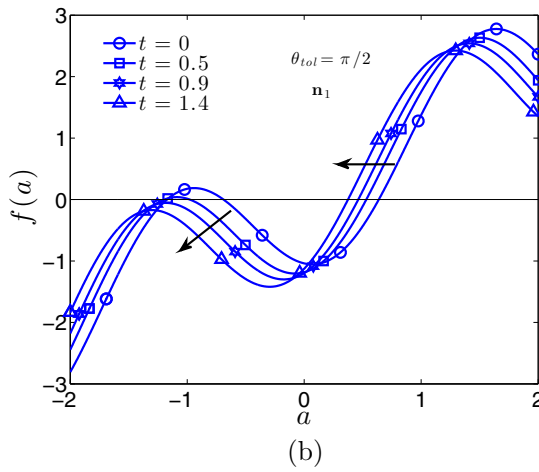
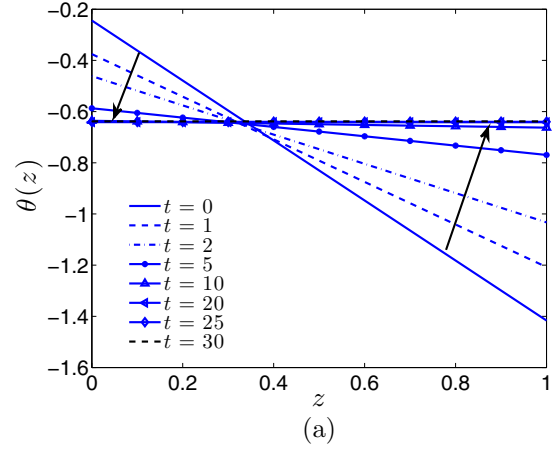
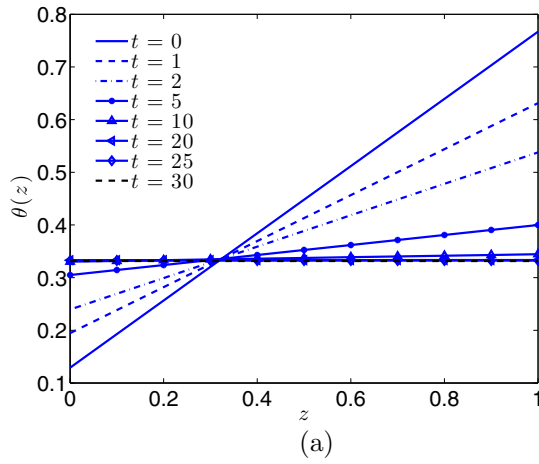


FIG. 6. (Color online) (a) The evolution of director solution \mathbf{n}_1 under gliding model I for $\alpha_0(0) = 0$, $\alpha_1(0) = \pi/3$, and $\theta_{tot} = \pi/2$. (b) The evolution of $f(a)$ under gliding (same parameters) when tracking \mathbf{n}_1 . Bistability is lost at $t \approx 0.6$. (c) The free energy $J(t)$ for \mathbf{n}_1 (solution tracked, solid curve) and \mathbf{n}_2 (“background” solution, dashed curve). The dashed curve stops where the background solution disappears.

background solution (its free energy at that point ceases to be a local minimum in the energy landscape and the solution disappears). Note that it is never the solution being tracked that disappears under gliding but always the other solution,

FIG. 7. (Color online) (a) The evolution of director solution \mathbf{n}_2 under gliding model I for $\alpha_0(0) = 0$, $\alpha_1(0) = \pi/3$, and $\theta_{tot} = \pi/2$. (b) The evolution of $f(a)$ under gliding (same parameters) when tracking \mathbf{n}_2 . Bistability is lost at $t \approx 2.5$. (c) The free energy $J(t)$ for \mathbf{n}_2 (solution tracked, solid curve) and \mathbf{n}_1 (“background” solution, dashed curve). The dashed curve stops where the background solution disappears.

resulting in a continuous evolution of a . The tracked solution always decreases its total free energy, becoming more stable with time, while the reverse applies to the background solution. Gliding model II leads to similar results: although the time

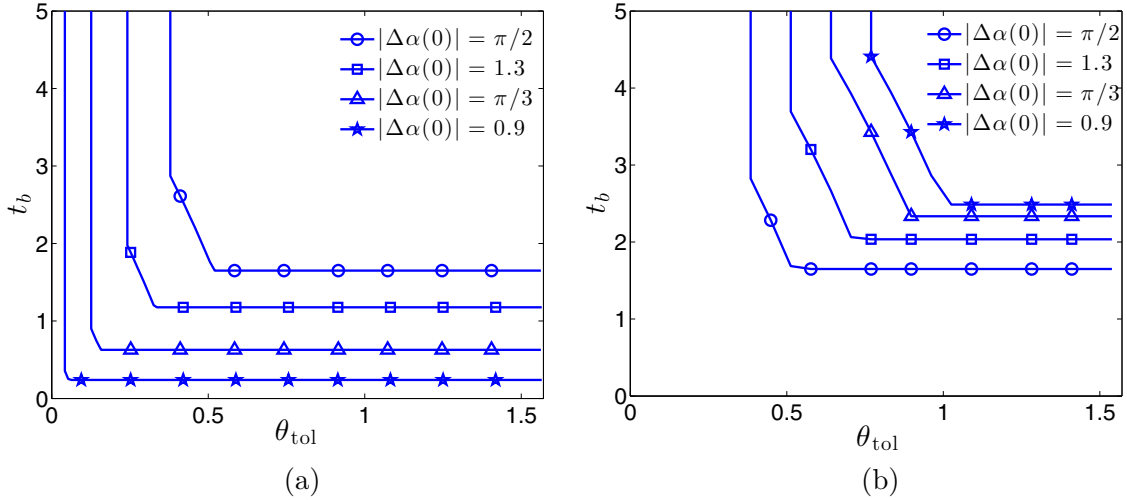


FIG. 8. (Color online) The time, t_b , at which bistability of a system is destroyed, vs θ_{tol} given a steady state \mathbf{n}_1 shown in (a) or \mathbf{n}_2 shown in (b) for various $\Delta\alpha(0) = \alpha_1(0) - \alpha_0(0)$ with $\alpha_0(0) = 0$. Gliding model I is used here.

at which bistability is destroyed varies slightly from gliding model I, it too ultimately destroys bistability provided that θ_{tol} is sufficiently large, as in model I.

2. Effect of limited gliding in model I

To determine how limited gliding, using model I, affects the structure of an initially bistable system in time, we solve Eqs. (7)–(10) for a range of values of θ_{tol} . Figure 8 shows the times t_b at which bistability is destroyed for different values of θ_{tol} and $\Delta\alpha(0)$. Both steady states \mathbf{n}_1 and \mathbf{n}_2 are considered separately. We first discuss the general properties of the behavior of the gliding system, and then we discuss the specific properties of each steady state separately. We observe that if θ_{tol} is small, then gliding lasts for a short time only, and the system will retain its bistability independently of which solution we track. In contrast, if θ_{tol} is sufficiently large, then the system will glide until bistability is destroyed. Figure 8 shows four different bistable cases, characterized by different values of $\Delta\alpha(0)$. While the results are quantitatively different between these four cases, three common key features are observed. First, if θ_{tol} is sufficiently small, then gliding always stops before bistability is destroyed, hence $t_b = \infty$. Second, if θ_{tol} is sufficiently large, then bistability will be lost before either anchoring angle has glided through the tolerance value; therefore, in such situations t_b is independent of θ_{tol} (the horizontal portions of the graphs). Third, the horizontal and vertical portions of the graphs are connected by intermediate sloped portions. These relate to situations in which, depending on the value of θ_{tol} and the initial anchoring conditions, gliding may stop first at one boundary but continue at the other, leading to the ultimate loss of bistability.

The transitions between the different portions of the $(\theta_{\text{tol}}, t_b)$ graphs depend on which solution is considered (\mathbf{n}_1 or \mathbf{n}_2) and on the initial state, characterized by $\Delta\alpha(0)$. Due to the special symmetry of the case, $\Delta\alpha(0) = \pi/2$, where \mathbf{n}_1 and \mathbf{n}_2 are simple mirror images, these two curves are the same in Figs. 8(a) and 8(b). However, for other values of $\Delta\alpha(0)$, the two corresponding steady states, \mathbf{n}_1 and \mathbf{n}_2 , give rise to different behavior. We find that, in line with our observations

about energetics in the unlimited gliding case at the end of Sec. III C 1, in general when tracking \mathbf{n}_2 we require larger values of θ_{tol} to destroy bistability (compare Figs. 6 and 7: the solution \mathbf{n}_1 is associated with a relatively deep free-energy minimum, and it takes longer to eliminate under gliding). Therefore, when tracking solution \mathbf{n}_2 , gliding must proceed for a longer time in order to eliminate the stable steady state \mathbf{n}_1 and destroy bistability, hence higher values of θ_{tol} are required for this to happen.

Since the number of steady states (at any given time) in an initially bistable system depends on both θ_{tol} and the difference in initial anchoring angles $\Delta\alpha(0)$, we now further investigate how $\Delta\alpha(0)$ influences bistability under gliding. We define $\theta_{\text{tol}}^{\text{min}}$ to be the smallest value of θ_{tol} that leads to the loss of bistability under gliding for each value of $\Delta\alpha(0)$. Figure 9 plots $\theta_{\text{tol}}^{\text{min}}$

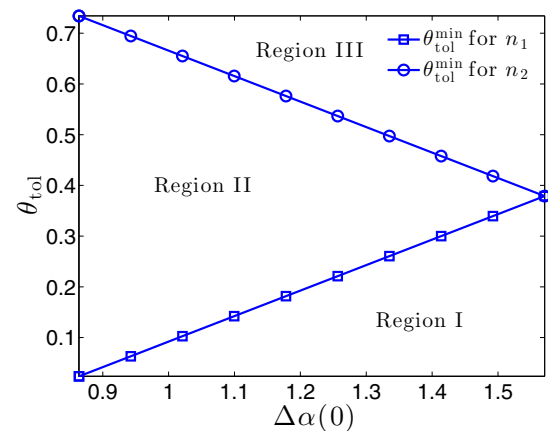


FIG. 9. (Color online) $\theta_{\text{tol}}^{\text{min}}$ (representing the smallest value of θ_{tol} that leads to loss of bistability under gliding) plotted as a function of $\Delta\alpha(0)$ for each steady state [\mathbf{n}_1 (\square) and \mathbf{n}_2 (\circ)]. These plots identify three regions in $(\theta_{\text{tol}}, \Delta\alpha(0))$ parameter space with initial steady states \mathbf{n}_1 and \mathbf{n}_2 : Region I: bistability is not destroyed regardless of which steady state is tracked; region II: bistability is lost when tracking \mathbf{n}_1 but not for \mathbf{n}_2 ; and region III: bistability is lost independently of which steady state we start from.

versus $\Delta\alpha(0)$ for both initial steady states \mathbf{n}_1 and \mathbf{n}_2 . We observe that $\theta_{\text{tol}}^{\text{min}}$ increases (very nearly linearly) with $\Delta\alpha(0)$ for \mathbf{n}_1 , but it decreases (again almost linearly) with $\Delta\alpha(0)$ for \mathbf{n}_2 . The two curves in Fig. 9 meet where $\Delta\alpha(0) = \pi/2$: this is again due to the mirror-image symmetry of \mathbf{n}_1 and \mathbf{n}_2 in this situation [with $\alpha_0(0) = 0$].

We can use these results to identify regions in $(\Delta\alpha(0), \theta_{\text{tol}})$ space where the system retains its bistability, depending on which director solution is tracked. With the chosen values of anchoring strengths and $\alpha_0(0) = 0$ we distinguish three such regions in Fig. 9: region I, in which bistability is never destroyed regardless of which steady state is tracked; region II, in which bistability is lost when tracking \mathbf{n}_1 but not when tracking \mathbf{n}_2 ; and region III, in which bistability is lost regardless of whether \mathbf{n}_1 or \mathbf{n}_2 is tracked.

3. Effect of limited gliding in model II

We now briefly outline the results analogous to those of Sec. III C 2 for gliding model II, Eqs. (7)–(9) and Eq. (11). Figure 10 (analogous to Fig. 8) shows the time t_b at which bistability is destroyed as a function of θ_{tol} . The behavior is qualitatively similar to that of model I, but smoothed. In the regions to the left of the nearly vertical portion of the curves, θ_{tol} is sufficiently small that bistability is never destroyed. When tracking \mathbf{n}_2 under gliding, larger values of θ_{tol} are needed to destroy bistability than when tracking \mathbf{n}_1 (see also Figs. 6 and 7). Also, for sufficiently large (but fixed) θ_{tol} , t_b decreases with $\Delta\alpha(0)$ for \mathbf{n}_1 and it increases as $\Delta\alpha(0)$ decreases for \mathbf{n}_2 . Again, the results for the symmetric case, $\Delta\alpha(0) = \pi/2$, in which \mathbf{n}_1 and \mathbf{n}_2 are mirror images, are identical in Figs. 10(a) and 10(b), as anticipated.

Unsurprisingly, models I and II generate quantitatively different results. Comparing the plots of t_b for \mathbf{n}_1 in both models [see Figs. 8(a) and 10(a)], we observe that when θ_{tol} is small, t_b is larger for model II, with the reverse trend for large θ_{tol} . Similarly, when tracking \mathbf{n}_2 in model II [see Fig. 10(b)], bistability is destroyed faster for large values of θ_{tol} and slower for small values of θ_{tol} [see Fig. 8(b)].

D. Effect of switching and unlimited gliding in a bistable system

Switching between the two stable steady states in an initially bistable system is possible in the absence of gliding [12,13]: with the application of a suitable transient electric field, one can achieve two-way switching in the appropriate parameter regimes. Motivated by the relevance of switching in devices that are both flexible and bistable, and by our results in Sec. III C, we now examine a bistable system in which both unlimited gliding ($\theta_{\text{tol}} = \pi/2$) and switching act sequentially, and we investigate the effect that such switching has on the system dynamics.

As an illustrative example, we consider an initially bistable system with anchoring conditions $\alpha_0(0) = 0, \alpha_1(0) = \pi/3$. As noted above, in practice two-way switching would be obtained through transient application of an electric field; however, in the present work, we simply impose the switch between states at specified times: we switch the system instantaneously from one stable state to the other by selecting the alternative (stable) root of Eq. (13) at the chosen switching time to obtain the new director solution (in any practical application, switching would occur on a time scale that is much faster than gliding, so from the point of view of the gliding dynamics this instantaneous switch is reasonable). Gliding is then continued, but now with the new steady state. For the example, illustrated in Fig. 11, we initially track \mathbf{n}_2 , and then we impose a series of switches at chosen switching times $t = 1, 2, 3, 4$, etc. Note that the initial steady state influences only the details of the results that follow; similar results are obtained if we initially track \mathbf{n}_1 .

Figure 11(a) shows the evolution of the director field over four successive switches. Figure 11(b) shows the evolution over many more successive switches, via the plot of the root, $a(t)$, of Eq. (13) that corresponds to the director solution being tracked under gliding, and via the corresponding total free energy $J(t) = J^*h^*/K^*$ [see Eq. (2)] of that solution. We observe that, in contrast to the case of unlimited gliding without switching, bistability is not destroyed, even though gliding occurs continuously throughout. If switching had not been imposed, then bistability would have been lost at $t_b \approx 2.3$; see Fig. 8.

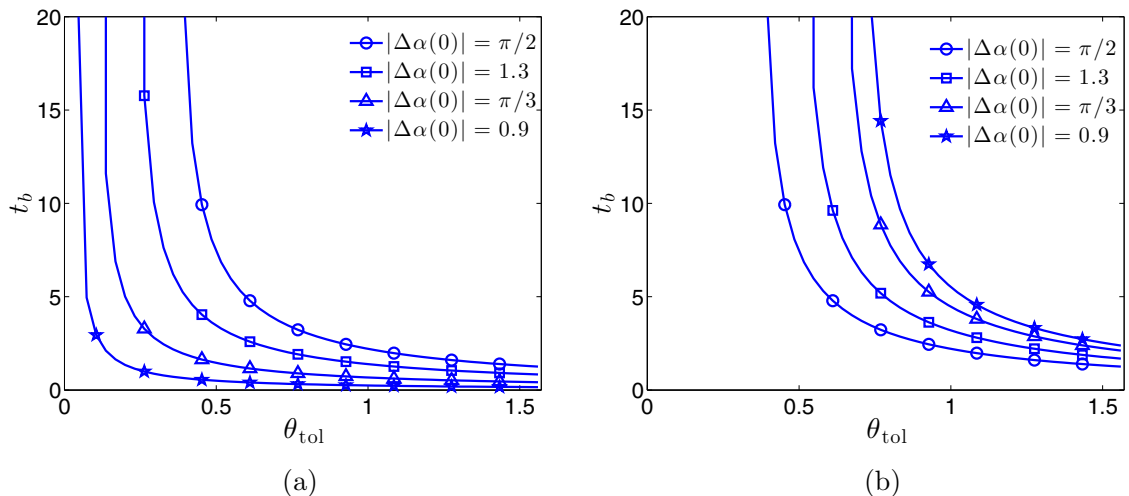


FIG. 10. (Color online) The time at which bistability of a system is destroyed, t_b vs θ_{tol} given a steady state \mathbf{n}_1 shown in (a) or \mathbf{n}_2 shown in (b) for various $\Delta\alpha(0)$ using gliding model II. Compare with Fig. 8 for model I.

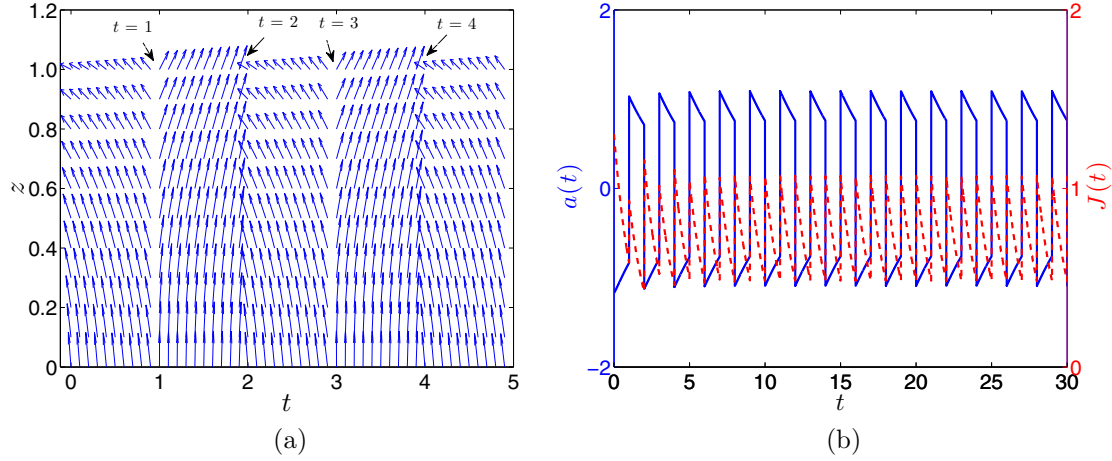


FIG. 11. (Color online) (a) Switching from $\mathbf{n}_2 \rightarrow \mathbf{n}_1 \rightarrow \mathbf{n}_2 \rightarrow \mathbf{n}_1 \rightarrow \mathbf{n}_2$ for $\alpha_0(0) = 0, \alpha_1(0) = \pi/3$ using gliding model I. (b) Switching and gliding dynamics for the same system over long times, monitored by plotting the selected root a (solid curve) of Eq. (12) and the free energy J (dashed curve) of the corresponding solution.

Figure 11(b) shows that, except at switching events, where energy is put into the system to make the switch, $|a(t)|$ (the total director bending angle across the layer) and $J(t)$ (the system free energy) are always decreasing under gliding, regardless of which state we track. The director is always relaxing toward a uniform state between switches, lowering its energy as it does so. However, recalling the results of Figs. 6 and 7, we know that as this happens, the “background” solution is simultaneously increasing its free energy.

Consider the behavior of $|a(t)|$ and $J(t)$ at the switching times $t = 1, 2, 3, 4, \dots, n$. At each switching time, both $|a(t)|$ and $J(t)$ jump (the states before and after the switch have different energies). Consider, for example, the switch from $\mathbf{n}_2 \rightarrow \mathbf{n}_1$ at $t = 2$. Here, $|a(2^+)| > |a(2^-)|$ (the \pm superscripts denote right- and left-handed limits, respectively), and $J(2^+) > J(2^-)$, indicating that (i) the solution after switching (\mathbf{n}_2 here) has a greater elastic bend across the layer than the solution before the switch (\mathbf{n}_1), and (ii) energy input is required to effect the switch (which in practice would most likely come from transient application of an electric field). Figure 11(b)

reveals that, although the initial behavior of the system is irregular, after many regularly spaced switches both $J(t)$ and $|a(t)|$ fall into a periodic behavior. This implies that regular switching can sustain bistability indefinitely: while gliding acts to dissipate elastic energy from the bulk, the act of switching puts new energy into the system. Providing that switching takes place sufficiently often, the bulk elastic energy can be maintained at a high enough level to retain the bistability. Another way to view this periodic behavior is that the regular switching reverses the effect of the gliding. Consider times $t = n$ sufficiently large that we are in the periodic regime. Immediately after a switch (to solution $\mathbf{n}_1|_{t=n^+}$, say) this solution begins to glide, evolving eventually to $\mathbf{n}_1|_{t=(n+1)^-}$. We can undo this gliding exactly if we now switch to solution $\mathbf{n}_2|_{t=(n+1)^+}$, allow it to glide for one time unit to $\mathbf{n}_2|_{t=(n+2)^-}$, and then switch to $\mathbf{n}_1|_{t=(n+2)^+} \equiv \mathbf{n}_1|_{t=n^+}$.

The example shown in Fig. 11 raises an interesting question: Since switching reverses the gliding effect in a bistable system, and we know that indefinite gliding with no switching leads inevitably to a loss of bistability, how often must we switch

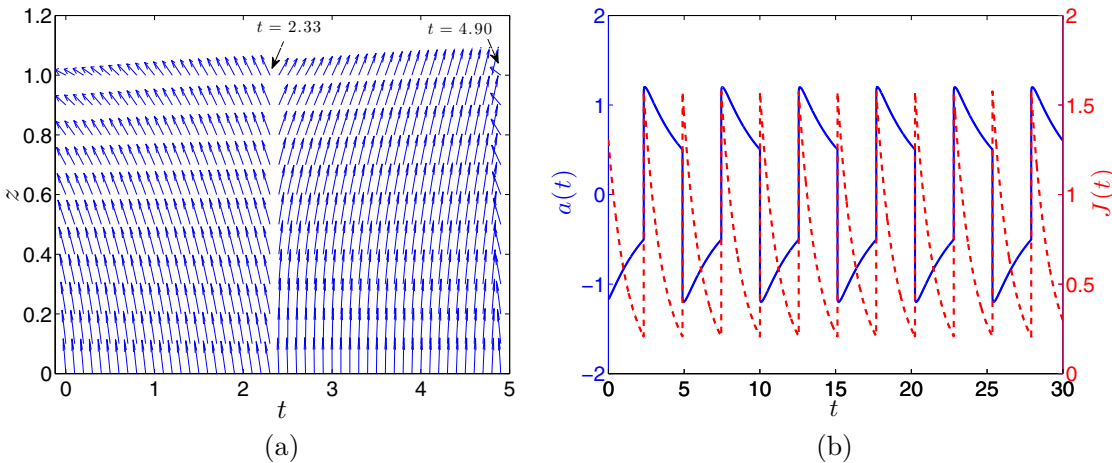


FIG. 12. (Color online) (a) Switching from $\mathbf{n}_2 \rightarrow \mathbf{n}_1 \rightarrow \mathbf{n}_2 \rightarrow \mathbf{n}_1$ for $\alpha_0(0) = 0$ and $\alpha_1(0) = \pi/3$ using gliding model I, with all switches imposed when the system is about to lose bistability. (b) Switching and gliding dynamics for the same system over long times, monitored by plotting the selected root a (solid curve) of Eq. (12) and the free energy J (dashed curve) of the corresponding solution.

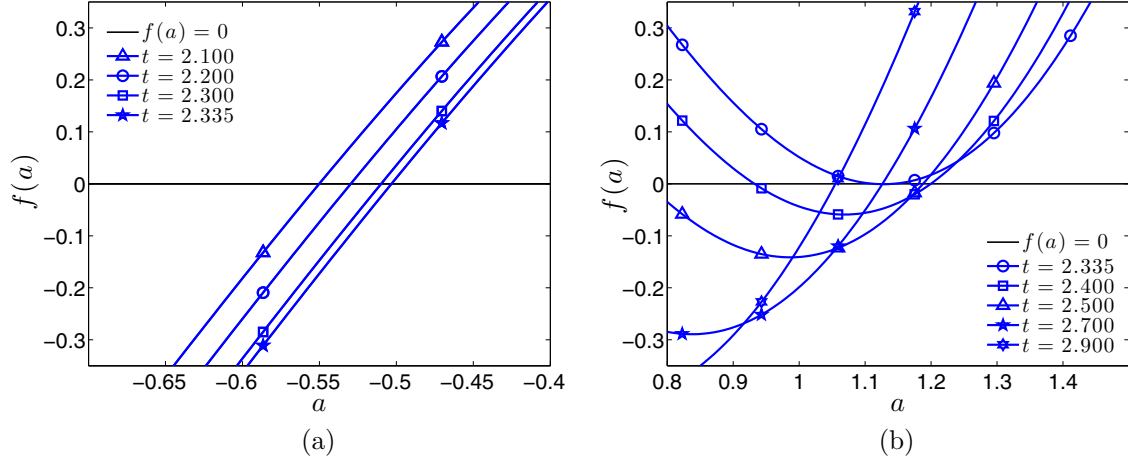


FIG. 13. (Color online) Evolution of $f(a)$, Eq. (13), close to the root and the switching time $t = 1.650$ from $n_2 \rightarrow n_1$ when $\alpha_0 = 0$, $\alpha_1(0) = \pi/3$. (a) Tracking the director configuration n_2 before switching at $t = 1.650$. (b) Tracking n_1 after switching at $t = 1.650$. The switch takes place just before bistability would have been lost.

to retain bistability? To answer this question (at least for our specific example), we modify the previous procedure: instead of switching between steady states at the chosen fixed times, we now let the system glide until it is about to lose bistability, then switch, ensuring that switching occurs at t_{lb} , which we define as the last time for which the system is bistable. Figure 12 shows an example of this procedure, applied repetitively. Figure 12(a) shows the director field, and Fig. 12(b) plots $a(t)$ and $J(t)$ as switching between the states occurs. As above, bistability can be maintained indefinitely with this approach. In addition, with this switching strategy we observe that $|a(t)|$ and $J(t)$ both fall into a periodic behavior immediately after the first switch occurs.

It is curious that this particular switching strategy changes the dynamics of the director solution immediately after the switch. For $t = t_{lb}^+$, $|a(t)|$ starts to *increase* briefly before the anticipated decrease under gliding. This behavior is reflected both in the plot of the director in Fig. 12(a) and in the plot of $a(t)$ in Fig. 12(b). Plotting the evolution of $f(a)$ before and after the first switching time $t_{lb} = 2.335$ (shown in Fig. 13), we observe that when tracking the initial solution n_2 , $f(a)$ (and the corresponding root) moves to the right [see Fig. 13(a)], while after switching to n_1 , $f(a)$ moves to the left and down [see Fig. 13(b)]. A transition phase occurs at $t = 2.335^+$ immediately following the switch where the root $|a(t)|$ continues to increase despite the change in evolution of $f(a)$ at the switch time [see the profiles of $f(a)$ at $t = 2.335$ and 2.400 in Fig. 13(b)]. Note, however, that, although this nonmonotone behavior of $a(t)$ under gliding immediately following switching is curious, the total energy following the switch immediately begins to decrease in time under the gliding, as anticipated.

Another interesting question to ask is how the energy lost due to gliding (compensated by the energy input in switching) depends on the switching interval, and whether there is an “optimum” switching strategy minimizing the total energy expenditure. To answer this question, we consider a general periodic switching strategy, and we compute the total energy lost due to gliding, $\Delta J_{n+1} = J(t)|_{t_n^+} - J(t)|_{t_{n+1}^-}$, for different

switching intervals $\Delta t = t_{n+1}^- - t_n^+$. Table I shows the total energy expenditure, $S_{\Delta J}$, for the period $t = 20$ to 100 , during which the system has settled into a periodic behavior. We observe that, at least for the case considered here, the total energy input needed to maintain bistability decreases as the time interval at which switching is applied increases (even though more energy is lost during each gliding cycle as its length increases). We conjecture that the most efficient approach to maintaining the bistability is to switch as late as possible.

Although in this section we have used specific examples to illustrate our results, we believe that certain conclusions apply quite generally. They are summarized as follows: (i) If an initially bistable system undergoes unlimited gliding, and no switching between states occurs, then a loss of bistability is inevitable (the system will approach a uniform director solution); (ii) if switching between the states is imposed sufficiently often (specifically, one must always switch to the “background” solution before it disappears), then bistability can be retained indefinitely; (iii) if the switching is imposed periodically, then the whole system will approach a periodic state at large times; and (iv) if we always wait the maximum time before switching (waiting until the background state is about to disappear), then the periodic behavior is attained immediately [possibly with some anomalous behavior in $a(t)$].

TABLE I. Total energy input as a result of switching measured from $t = 20$ until $t = 100$.

Total Energy Input vs Switching Interval	
Switching Interval	$S_{\Delta J}$
$t = 0.5$	47.34
$t = 1.0$	46.79
$t = 1.5$	44.71
$t = 2.0$	44.58
$t = 2.3$	42.67
$t = t_{lb}$	42.39

Finally, we remark that these examples and observations represent a worst-case scenario in which gliding is unlimited, so that a loss of bistability is inevitable with no switching. The introduction of limited gliding, $\theta_{\text{tol}} < \pi/2$, will only improve matters since, as we already know, if θ_{tol} is sufficiently small, then bistability can be retained indefinitely even with no switching.

IV. CONCLUSIONS

We have presented two models (I and II) that describe the evolution of the director field within a confined layer of a nematic liquid crystal, bounded by two infinite polymeric plates, where the anchoring is weak at both plates. At these plates, director gliding may occur: the anchoring angle or easy axis undergoes a continuous realignment under the torque due to the bulk elasticity of the nematic layer. In model I, gliding occurs at a rate proportional to the difference between the anchoring angle and the director angle at the interface considered, but it stops abruptly once the deviation of the anchoring angle from its initial value reaches some tolerance value, θ_{tol} (abrupt cessation). In model II, gliding is halted smoothly as θ_{tol} is approached (smooth cessation). Both models exploit the separation in time scales between gliding (long time scale) and elastic response (short time scale) to justify a quasistatic approximation for the director field orientation within the layer, with the model dynamics driven

purely by the gliding. We investigate in detail how director gliding, governed by each model, affects the evolution of the director field, as θ_{tol} and the initial anchoring angles vary. For large θ_{tol} , gliding leads to a director solution that is uniform throughout the domain for both gliding models.

We pay particular attention to the behavior under gliding of an initially bistable system. For large values of θ_{tol} , gliding destroys bistability independently of the model chosen. However, the time at which bistability is destroyed is model-dependent. Furthermore, we investigate how switching between stable steady states, in the presence of gliding, can affect the number of available steady states at a given time. We conclude that switching can retain bistability, even under unlimited gliding, as long as it occurs sufficiently often. Furthermore, we find that if retention of bistability is the sole aim, then it is advantageous to switch as late as possible (just before the system is about to lose bistability): such a strategy minimizes the energy lost due to gliding.

We expect that the models proposed here will provide an appropriate foundation for considering more realistic switching driven by an applied electric field, combined with gliding. This will be the subject of our future work.

ACKNOWLEDGMENTS

Financial support from NSF under Grant No. DMS-1211713 is gratefully acknowledged.

-
- [1] *Advances in Display Technologies; and E-Papers and Flexible Displays*, edited by K. Blankenbach, L.-C. Chien, S.-D. Lee, and M. H. Wu, Proc. SPIE Vol. 7956 (2011).
 - [2] P. Palffy-Muhoray, The diverse world of liquid crystals, *Phys. Today* **60**(9), 54 (2007).
 - [3] A. J. Davidson and N. J. Mottram, Flexoelectric switching in a bistable nematic device, *Phys. Rev. E* **65**, 051710 (2002).
 - [4] P. Yeh and C. Gu, *Optics of Liquid Crystal Displays* (Wiley, New Jersey, 2009).
 - [5] I. Jánossy, Kinetics of director gliding on a polymer liquid-crystal interface, *Phys. Rev. E* **81**, 031714 (2010).
 - [6] I. Jánossy and T. I. Kósa, Gliding of liquid crystals on soft polymer surfaces, *Phys. Rev. E* **70**, 052701 (2004).
 - [7] S. Joly, K. Antonova, P. Martinot-Lagarde, and I. Dozov, Zenithal gliding of the easy axis of a nematic liquid crystal, *Phys. Rev. E* **70**, 050701 (2004).
 - [8] P. Vetter, Y. Ohmura, and T. Uchida, Study of memory alignment of nematic liquid crystals on polyvinyl alcohol coatings, *Jpn. J. Appl. Phys.* **32**, L1239 (1993).
 - [9] V. P. Vorflusev, H. Kitzerow, and V. G. Chigrinov, Azimuthal surface gliding of a nematic liquid crystal, *Appl. Phys. Lett.* **70**, 3359 (1997).
 - [10] S. Faetti, M. Nobili, and I. Raggi, Surface reorientation dynamics of nematic liquid crystals, *Eur. Phys. J. B* **11**, 445 (1999).
 - [11] S. Pasechnik, V. Chigrinov, D. Shmeliova, V. Tsvetkov, V. Kremenetsky, L. Zhijian, and A. Dubtsov, Slow relaxation processes in nematic liquid crystals at weak surface anchoring, *Liq. Cryst.* **33**, 175 (2006).
 - [12] L. J. Cummings and G. Richardson, Bistable nematic liquid crystal device with flexoelectric switching, *Eur. J. Appl. Math.* **17**, 435 (2006).
 - [13] L. J. Cummings, C. Cai, and L. Kondic, Towards an optimal model for a bistable nematic liquid crystal display device, *J. Eng. Math.* **80**, 21 (2013).
 - [14] P. Kedney and F. Leslie, Switching in a simple bistable nematic cell, *Liq. Cryst.* **24**, 613 (1998).
 - [15] M.-C. Choi, Y. Kim, and C.-S. Ha, Polymers for flexible displays: From material selection to device applications, *Prog. Polym. Sci.* **33**, 581 (2008).
 - [16] J. S. Gwag, J. Kim, M. Yoneya, and H. Yokoyama, Surface nematic bistability at nanoimprinted topography, *Appl. Phys. Lett.* **92**, 153110 (2008).
 - [17] I. Jánossy, High-precision measurement of azimuthal rotation of liquid crystals on solid substrates, *J. Appl. Phys.* **98**, 043523 (2005).
 - [18] P. G. De Gennes and J. Prost, *The Physics of Liquid Crystals* (Oxford University Press, New York, 1995).
 - [19] S. Chandrasekhar, *Liquid Crystals* (Cambridge University Press, Cambridge, 2007).
 - [20] A. Rapini and M. Papoular, Distorsion d'une lamelle nématique sous champ magnétique, conditions d'ancrage aux parois, *J. Phys. (Paris, Colloq.)* **30**, 54 (1969).
 - [21] F. Leslie, Theory of flow phenomena in liquid crystals, *Adv. Liq. Cryst.* **4**, 1 (1979).
 - [22] G. E. Durand and E. G. Virga, Hydrodynamic model for surface nematic viscosity, *Phys. Rev. E* **59**, 4137 (1999).